RSC Advances

PAPER

View Article Online
View Journal | View Issue

Cite this: *RSC Adv.*, 2025, **15**, 27026

Preparation and printing optimization of an organic carrier for silver paste on the front side of solar cells

Yongqing Hu,[ad] Yibo Huang,[ad] Lei Li,[bde] Jiqiang Gao,[bde] Kai Zhou,[bde] Liang Fang*[c] and Hu Sun*[bde]

Received 27th May 2025
Accepted 9th July 2025

DOI: 10.1039/d5ra03728j

rsc.li/rsc-advances

The rheological properties and screen-printing behavior of silver paste on the front side of solar cells are critical for achieving high-resolution electrode patterns. This study investigates the viscosity and thixotropy of organic carriers, analyzes the screen printing performance of conductive silver paste, and systematically examines the key factors affecting grid line formation. The results indicate that shorter ethyl cellulose chains reduce the silver paste viscosity under high shear rates, enhancing its suitability for screen printing. The addition of 1 wt% polyamide wax to the organic carrier yields optimal thixotropic recovery. During the fine-line printing process, the speed and downward pressure of the squeegee affect the width and height of the grid lines. Ultimately, an organic carrier formulation with excellent thixotropic and rheological properties was developed.

1. Introduction

In solar cells, silver grid lines are screen-printed onto silicon wafers to facilitate electron collection and conduction, with their performance critically dependent on the quality of the front-side silver paste.[1] Although the organic vehicle constitutes merely 5–15% of the front-side silver paste composition, it governs the paste's rheological behavior and printability,[2–4] thereby exerting a profound influence on both electrode fabrication and electrical performance.[5] The rheological properties of the silver paste—particularly its shear-thinning pseudoplasticity and thixotropy—are essential for ensuring uniform flow through the screen mesh and the formation of well-defined grid line patterns.[6–8] Grid line shading loss is a dominant factor limiting the photoelectric conversion efficiency of front-side silver electrodes in solar cells. Reducing the grid line width minimizes sunlight obstruction and enhances light absorption. However, maintaining low series resistance simultaneously requires increasing grid line height—i.e., achieving a high aspect ratio. Excessively narrow grid lines may result in irregular or discontinuous printed electrodes, ultimately degrading the solar cell's power conversion efficiency.[9–11] Consequently, screen-printing processes must precisely control the morphological integrity and aspect ratio of the grid lines to optimize the trade-off between optical loss minimization and electrical performance preservation. To achieve high-aspect-ratio grid lines, the silver paste must demonstrate high viscosity at low shear rates (ensuring shape retention) and low viscosity at high shear rates (enabling smooth extrusion through fine screen openings). This dual requirement—manifested as pronounced thixotropy and rapid structural recovery—mitigates printing defects such as incomplete transfer or line breakage, reduces screen clogging, and enhances printing efficiency.[12] Such performance hinges on both the paste's rheological properties and advancements in screen-printing technology.[13] For example, recent developments in knot-free screens have reduced opening widths below 20 μm,[14] imposing stricter demands on paste formulation. In addition to developing new screen printing plates, researchers currently employ more advanced printing technologies such as plating[15] and nanoimprint lithography[16] to achieve fine grid line printing. Although these methods can achieve higher aspect ratios, they also entail significantly higher production costs. In this study, through systematic optimization of screen-printing parameters, we successfully fabricated silver electrodes with a width of 18.68 μm, a height of 9.44 μm, and an aspect ratio of 0.50—all while maintaining cost-effectiveness.

Ethyl cellulose is widely used in the industry due to its favorable printability and leveling characteristics.[17] It induces complex rheological responses by interacting with the slurry through surface affinity and hydrogen bonding.[18] Thixotropic behavior in organic carriers is primarily imparted by thixotropic agents. Thixotropy allows the slurry to thin under shear and recover viscosity upon rest, enabling high aspect ratios during

[a]*Kunming Institute of Precious Metals, Yunnan Province, 650032, People's Republic of China*

[b]*Sino-Platinum Metals Co., Ltd, Yunnan Province, 650106, People's Republic of China. E-mail: sunhu@ipm.com.cn*

[c]*China Zhenhua Group Yunke Electronics Co., Ltd, Guizhou Province, 550018, People's Republic of China. E-mail: zhiyx2022@163.com*

[d]*State Key Laboratory of Precious Metal Functional Materials, Yunnan Province, 650106, People's Republic of China*

[e]*Sino-Platinum Electronic Materials (Yunnan) Co. Ltd, Yunnan Province, 650503, People's Republic of China*

screen printing. Excellent thixotropy in the carrier ensures that the slurry exhibits similar rheological behavior. This ensures that the printed silver lines retain a favorable aspect ratio during the printing process.[19] This work formulates an organic carrier by examining ethyl cellulose and thixotropic agent, resulting in high yield stress, strong thixotropy, and rapid recovery. Additionally, the effects of viscosity, thixotropy, and printing parameters on the aspect ratio of silver grid lines are discussed. This study aims to inform and optimize silver paste printing for solar cell applications.

2. Experimental

2.1 Organic carrier and silver paste preparation

The organic solvents and thickeners in each formulation were precisely weighed using an electronic balance and mixed in a clean beaker. A magnetic stir bar of appropriate size was added to the beaker, which was then sealed with plastic film to minimize solvent evaporation during preparation. The beaker was placed in a thermostatic magnetic stirring water bath, with the stirring speed set to 300 rpm and the temperature maintained at 80–90 °C. Once the thickener was fully dissolved, the bath temperature was lowered to 60 °C, followed by the addition of surfactants (lecithin and Span 85) and thixotropic agents (hydrogenated castor oil and polyamide wax). After complete dissolution, the mixture was stirred at 60 °C for 1 hour to obtain the organic carrier. The organic carrier was mixed with glass powder and silver powder in the specified proportions. The three components were pre-mixed in an agate mortar until fully wetted, forming a non-Newtonian silver paste. The pre-mixed silver paste was processed 3–5 times using a three-roll mill.[20,21]

2.2 Silver paste viscosity

The effects of different ethyl cellulose models (EC4, EC10, EC20, EC100) and their concentrations on the viscosity of the silver paste were investigated.[22] Among these models, "EC" denotes the series abbreviation, while the numerical values indicate the viscosity of ethyl cellulose (measured in mPa s). The viscosity is typically determined under standardized conditions, using a 5% (w/w) ethyl cellulose solution in a toluene/ethanol (80 : 20 v/v) solvent mixture at 25 °C. A higher numerical value corresponds to greater viscosity, reflecting longer molecular chains and a higher degree of polymerization. The degrees of polymerization of ethyl cellulose used in this study were 15, 60, 100, and 500 in ascending order. Ethyl cellulose was mixed with organic solvents at concentrations of 2 wt%, 4 wt%, 6 wt%, 8 wt%, and 10 wt% to prepare organic carriers. Rheological curves were obtained using a rheometer to identify organic carriers with suitable viscosity ranges.[23] The selected organic carrier (10 wt%) was blended with silver powder and glass powder to formulate the silver paste. The rheological properties of the organic carrier and silver paste were measured using a rheometer (RST-SST, BROOKFIELD) equipped with a 25 mm diameter lower plate and a 1° upper cone at 25 °C.[24,25] Before each test, the silver paste was allowed to stand for 3 minutes to minimize the memory effect from the initial shear loading.[26] Steady shear flow tests were conducted over a shear rate range of 0.1–1000 s^{-1} to measure viscosity and construct viscosity-shear rate curves based on the acquired data.[27] A three-interval thixotropy test (3lTT) under constant shear strain was conducted to simulate slurry behavior during screen printing.[28] In the first interval, representing the pre-printing stage, the cone shear rate was maintained at 1 s^{-1} for 80 seconds. In the second interval, a high shear rate of 200 s^{-1} was applied for 28 seconds to simulate the scraper movement during printing. During the third interval, the shear rate was reduced back to 1 s^{-1} to evaluate the structural recovery of the silver paste.[29] To identify the optimal silver paste formulation for printing fine grid lines on solar cell front electrodes, a semi-automatic screen printing machine was used under consistent conditions to apply the paste to c-Si solar cells. A custom-designed front electrode mesh screen was used, featuring 430 mesh count, 7 μm emulsion thickness, 15 N tension, and a gate opening width of 23 μm. The continuity and linearity of the printed silver grid lines were examined using a polarized light microscope and an optical lens.

2.3 Silver paste thixotropy performance

The thixotropic behavior of silver paste primarily originates from its organic carrier. To investigate the effect of different thixotropic agents on carrier thixotropy, hydrogenated castor oil and polyamide wax were employed as independent variables in the organic carrier formulations. The detailed formulations of the organic carriers are provided in the table below (Table 1).

Thixotropic behavior was evaluated using rheological hysteresis loops, which assess the viscosity recovery rate after shear deformation. A rheometer was used to perform continuous shear tests on four organic carriers. The shear rate was increased from 1 s^{-1} to 100 s^{-1} over 0–100 seconds to obtain the shear-thinning curve. Subsequently, from 100 to 200 seconds, the shear rate was decreased from 100 s^{-1} to 1 s^{-1} following the same rate as the acceleration phase, yielding the thixotropic recovery curve.[30]

2.4 Printing process

The width and aspect ratio of the grid lines are not exclusively governed by the rheological properties of the silver paste or

Table 1 Formulation table of the organic carrier for different thixotropic agents

Organic carrier sample	Ethyl cellulose EC10	Hydrogenated castor oil	Polyamide wax	Organic solvent	Other
OC 1	10	1	0	80	9
OC 2	10	1.5	0	79.5	9
OC 3	10	0	1	80	9
OC 4	10	0	1.5	79.5	9

Table 2 Printing parameters of the sample

Sample	Scraper speed (cm s^{-1})	Scraper downforce (N)	Screen opening (μm)	Screen tension (N)	Film thickness (μm)
SP 1	5	10	14	20	7
SP 2	5	30	14	20	7
SP 3	25	10	14	20	7
SP 4	25	30	14	20	7

screen-printing parameters, highlighting the need for a systematic investigation into the influence of the printing process parameters on silver paste deposition. During the fabrication of silver electrodes, empirical observations revealed that even with identical screen configurations and paste formulations, variations in squeegee pressure and movement speed significantly altered the grid line morphology. Excessive squeegee pressure induced ink bleeding, whereas insufficient pressure resulted in incomplete paste transfer. Additionally, the squeegee speed exhibited an inverse relationship with the deposited paste volume. Based on preliminary optimization trials, the printing parameters detailed in Table 2 were selected, and samples SP1–SP4 were fabricated using silver paste Poc6. To evaluate the printed grid line morphology, longitudinal cross-sections were characterized *via* scanning electron microscopy (SEM), enabling quantitative analysis of aspect ratios and qualitative assessment of structural uniformity.

3. Results and discussion

3.1 The influence of thixotropic agents on the thixotropy of organic carriers

As shown in Fig. 1, the organic carrier OC3 demonstrates the best thixotropic behavior and recovery performance. Analysis indicates that polyamide wax exhibits superior thixotropic properties compared to hydrogenated castor oil, suggesting that it forms more stable thixotropic structures within the organic carrier. This is attributed to its ability to form more hydrogen bonds with ethyl cellulose, enabling rapid thinning under shear and resulting in lower flow viscosity. Moreover, polyamide wax facilitates faster hydrogen bond reformation, allowing rapid viscosity recovery upon shear rate reduction. In this system, 1 wt% polyamide wax exhibited superior thixotropic recovery compared to 1.5 wt%. Therefore, 1 wt% polyamide wax was selected as the thixotropic agent for the organic carrier.

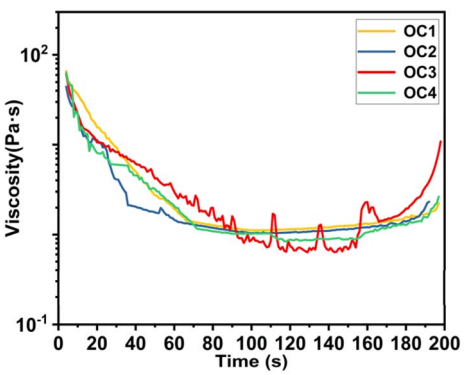

Fig. 1 Thixotropic recovery curves of four different thixotropic agent organic carriers.

3.2 The effect of viscosity on the printing performance of silver paste

As shown in Fig. 2, the viscosity-shearing ratio analysis of organic carriers with different ethyl cellulose contents was performed. All organic carriers exhibited pseudoplastic behavior of shear thinning, and the viscosity of the organic carrier increased significantly with the increase of the ethyl cellulose content. Fig. 2 shows that when the ethyl cellulose content exceeds 8 wt%, the shear thinning effect of the organic carrier is better, resulting in a lower viscosity at a high shear rate, thereby improving the printing performance of the silver paste. However, as the content of ethyl cellulose decreases, the viscosity decrease at high shear rate may decrease, potentially weakening pseudoplasticity due to insufficient network formation at low cellulose levels. Additionally, to ensure the silver paste achieves a solid content above 90 wt% for high post-sintering conductivity, a moderate organic carrier viscosity is required. Excessively high viscosity hinders slurry preparation, with static viscosity typically maintained around 50 Pa s. Therefore, organic carriers containing 8 wt% EC4, 10 wt% EC10, 8 wt% EC10, and 6 wt% EC20 were selected for further investigation (Table 3).

The organic carriers OC5 to OC8 correspond to silver pastes Poc5 to Poc8. As shown in Fig. 3(a), the silver pastes exhibit higher viscosity at low shear rates, which enhances stability on the screen prior to printing and prevents flow or dripping. At high shear rates, their viscosity decreases significantly, facilitating smooth screen printing and paste leveling, attributed to the disruption of hydrogen bonds and rapid breakdown of the internal network structure. During the recovery phase, viscosity gradually increases, indicating the reformation of internal hydrogen bonds and the structural network, which supports rapid line shaping and minimizes edge diffusion or collapse after printing. Ultimately, the relatively high viscosity of the silver paste helps prevent overflow during screen printing and ensures the dimensional accuracy of the grid lines. Among the samples, Poc6 demonstrates an ideal balance high low-shear viscosity and the lowest viscosity at high shear rates. Fig. 3(b) compares the viscosity recovery rates of silver pastes with different organic carriers. Poc5 recovered 80% of its low-shear viscosity within 14 seconds and Poc6 recovered over 95% within just 4 seconds. Although Poc7 and Poc8 were slightly

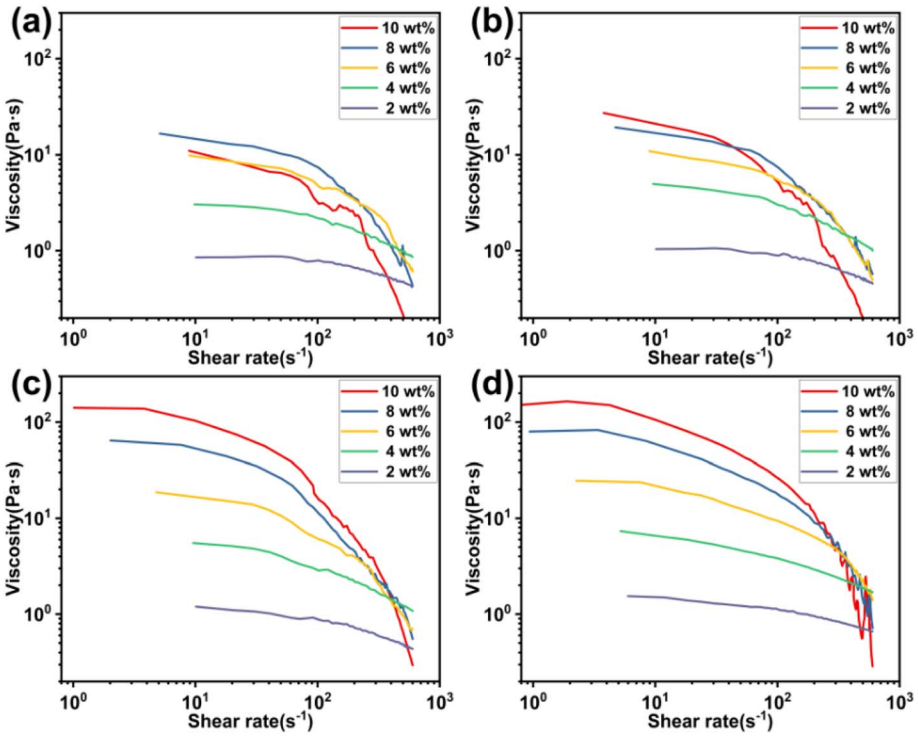

Fig. 2 (a) Adhesive shear curve of the organic carrier with different content of EC4, (b) adhesive shear curve of the organic carrier with different content of EC10, (c) adhesive shear curve of the organic carrier with different content of EC20 and (d) adhesive shear curve of the organic carrier with different content of EC100.

slower, both still achieved 80–90% recovery. These results suggest that longer molecular chains and higher polymerization levels of ethyl cellulose hinder the achievement of low viscosity at high shear rates, whereas shorter molecular chains with lower polymerization impair the rapid viscosity recovery of silver paste after shear. Consequently, Poc6 demonstrates the best overall performance featuring ideal low-shear viscosity, minimal high-shear viscosity and excellent viscosity recovery.

Table 3 Formulation table of different ethyl cellulose organic carriers

Organic carrier sample	Ethyl cellulose EC4	Ethyl cellulose EC10	Ethyl cellulose EC20	Polyamide wax	Organic solvent	Other
OC 5	8	0	0	1	82	9
OC 6	0	8	0	1	82	9
OC 7	0	10	0	1	80	9
OC 8	0	0	6	1	84	9

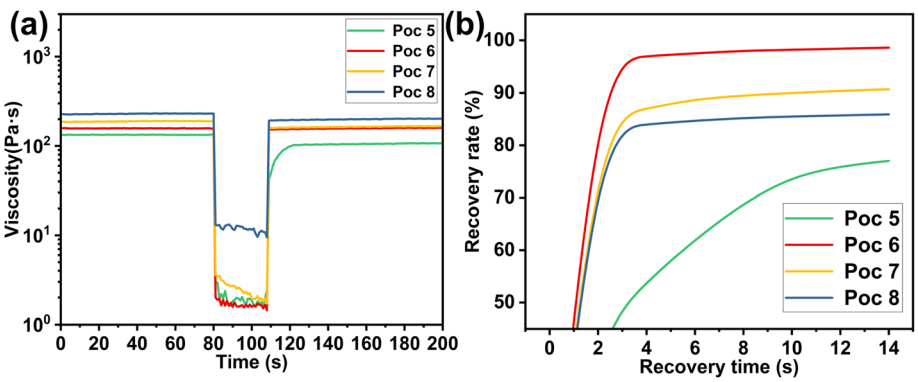

Fig. 3 (a) 3ITT test curve of constant shear strain of silver paste and (b) curve of viscosity recovery rate and recovery time of silver paste.

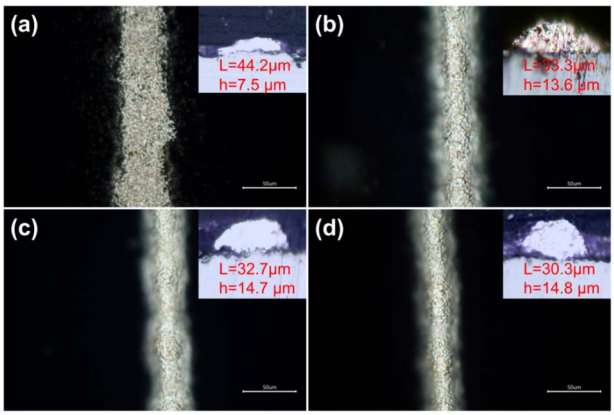

Fig. 4 Grout printing grid line optical microscope image (a) Poc5, (b) Poc6, (c) Poc7 and (d) Poc8.

Fig. 4 presents optical microscope images of the surface and cross-sections of the silver grid lines after printing and sintering with four different silver pastes. Fig. 4(a) shows the Poc5-printed sample, featuring a very flat grid line surface but a relatively wide line and low height. Fig. 4(b) and (c) display samples printed with Poc6 and Poc7, respectively, both showing similar surface morphology. However, due to the slightly higher viscosity of Poc7, its aspect ratio is marginally greater than that of Poc6. Fig. 4(d) shows the Poc8-printed sample, with an aspect ratio of 0.49. As previously discussed, the poor viscosity recovery of Poc5 after high shear prevented it from quickly regaining structure post-printing, leading to silver paste spreading and a significantly reduced aspect ratio. While Poc6 exhibits similar performance to Poc7, its superior thixotropy and recovery behavior allow for the printing of thinner, more refined grid lines. Cross-sectional analysis shows that grid lines printed with Poc6 are more regular and uniform. Due to its high viscosity, Poc8 produces a grid line with a high aspect ratio close to 0.5, but exhibits line breakage, as shown in Fig. 5. Its poor thixotropy and elevated viscosity impede the paste's ability to pass through the screen, resulting in printing defects such as line discontinuities and dummy areas. These defects negatively impact the conductivity of the silver electrodes, making Poc8 unsuitable for use in front-electrode silver pastes for c-Si solar cells.

3.3 Influence of silver paste printing parameters on grid line formation

The longitudinal cross-section of sample SP1 (Fig. 6(a)) shows a line width of 23.76 μm, height of 8.12 μm, and aspect ratio of 0.34. Fig. 6(b) shows sample SP2, with a line width of 18.05 μm, height of 7.78 μm, and aspect ratio of 0.43. Fig. 6(c) displays sample SP3, with a width of 23.23 μm, height of 9.62 μm, and aspect ratio of 0.41. Sample SP4, shown in Fig. 6(d), has a grid line width of 18.68 μm, height of 9.44 μm, and aspect ratio of 0.50. The electrical performance of the grid lines fabricated from the four sample sets is summarized in Table 4. The results indicate that samples with higher aspect ratios demonstrate significantly lower series resistance (R_s), with SP4 exhibiting the lowest R_s value of 1.44 mΩ. This improvement can be attributed to the reduced width of high-aspect-ratio grid lines at a constant cross-sectional area, which minimizes shading losses and consequently enhances conductivity by lowering R_s. This study also reveals that increasing the scraper speed results in a higher grid line height; whereas higher scraper pressure causes the line width to approach that of the screen opening. However, excessive scraper speed can prevent proper adhesion of the paste to the silicon wafer, leading to defects such as dummy lines and breakage. In this study, the selected scraper speed of 25 cm s^{-1} remained within the acceptable range. When the scraper pressure exceeded 30 N, a further reduction in line width was not observed, and excessive force risked damaging the c-Si solar cells.

The screen printing process is as follows. First, an appropriate amount of silver paste is placed on the screen mesh at the leading edge of the scraper. The filling scraper then moves at a preset speed in the opposite direction of printing, without applying downward pressure, to fill the screen openings. Next,

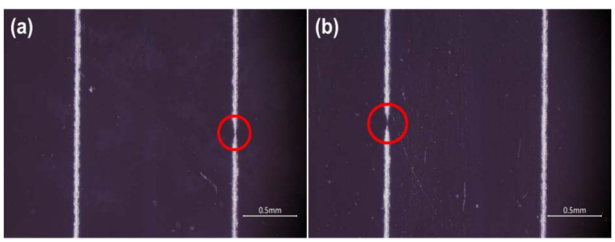

Fig. 5 Micrographs of discontinuous finger interruptions at different printing positions for Poc8 paste: (a) position 1; (b) position 2.

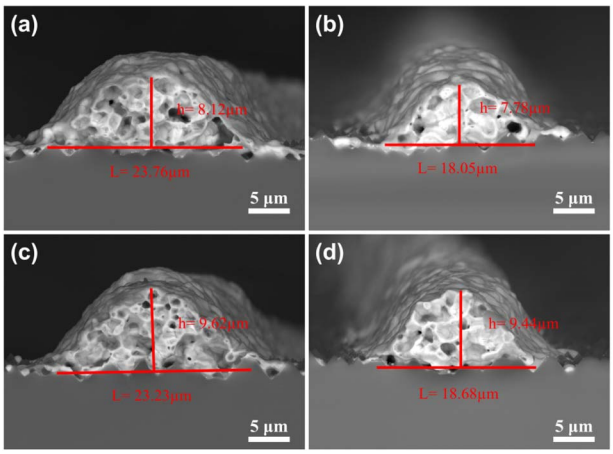

Fig. 6 SEM diagram of the grid line longitudinal section: (a) sample SP1, (b) sample SP2, (c) sample SP3 and (d) sample SP4.

Table 4 The electrical performance data for the three pastes

Sample	Width (μm)	Height (μm)	Aspect ratio (μm)	R_s (mΩ)
SP1	23.76	8.12	0.34	1.67
SP2	18.05	7.78	0.43	1.56
SP3	23.23	9.62	0.41	1.52
SP4	18.68	9.44	0.50	1.44

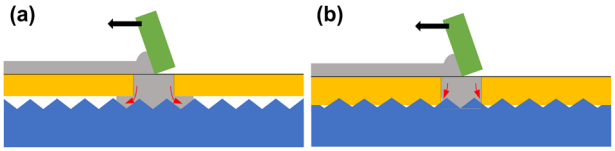

Fig. 7 (a) Schematic diagram of the contact between the grid and c-Si solar cells when the lower pressure of the scraper is small. (b) Schematic diagram of the contact between the grid and c-Si solar cells when the lower pressure of the scraper is large.

the printing scraper moves in the printing direction at a set speed and angle, applying constant downward pressure to bring the screen into contact with the surface of the c-Si solar cell. This action allows the silver paste to transfer to the substrate through the screen openings. As the scraper passes over the screen, the tension in the mesh causes it to rebound, lifting away from the substrate and returning to its original position, leaving behind the printed pattern on the c-Si solar cell. The scraper movement speed determines the rebound rate of the mesh. A slower printing speed results in a slower mesh rebound, allowing the silver paste sufficient time to recover its internal thixotropic structure. This enhances cohesion and prevents the mesh from pulling the grid line upward. In contrast, during fast printing, the mesh rebounds quickly before the paste fully recovers its viscosity, leading to stretching of the grid line and increased line height. Therefore, higher scraper speeds contribute to greater grid line height.

Fig. 7 provides a schematic of the contact between the screen and the c-Si solar cell during screen printing. When the scraper pressure is low, insufficient contact occurs between the screen and the silicon wafer. As a result, the low viscosity paste under high shear spreads through the gap, leading to an increased grid line width (Fig. 7(a)). In contrast, higher scraper pressure ensures close contact between the mesh and the wafer, limiting paste diffusion (Fig. 7(b)). Therefore, sufficient downward pressure ensures that the printed line width closely matches the screen opening. Consequently, sample SP4 achieves the narrowest grid line width and the highest aspect ratio among the tested conditions.

4. Conclusions

In this study, the characteristics of ethyl cellulose and thixotropic agents were thoroughly investigated, leading to the successful development of a novel organic carrier formulation. The optimized formulation exhibits high yield stress, excellent thixotropic behavior and rapid structural recovery after shear. The results indicate that the thixotropy of the silver paste is primarily governed by the type and concentration of thixotropic agents. In particular, polyamide wax outperforms hydrogenated castor oil in forming thixotropic structures. The ethyl cellulose content significantly influences the viscosity of the organic carrier at both high and low shear rates. However, the optimal concentration must be maintained—excessive or insufficient content can adversely affect the formulation and printability of the silver paste. Among the tested formulations, the organic carrier with 8 wt% EC10 exhibited optimal rheological behavior, producing silver paste with excellent screen-printing characteristics. Furthermore, printing parameters were found to significantly affect the geometry of the printed grid lines. Specifically, the study found that increasing the squeegee speed elevates the line height, which is attributed to the faster rebound speed of the screen mesh before the silver paste fully recovers its viscosity. Meanwhile, increasing the squeegee pressure promotes tighter contact between the screen and substrate, thereby improving the pattern definition. Through comprehensive optimization of the printing process parameters, we achieved the dual objectives of line width reduction and aspect ratio enhancement while employing conventional cost-effective screen printing technology and standard screens, thus obtaining qualified products at low cost. After optimizing the organic vehicle formulation and printing process parameters (squeegee speed = 25 cm s^{-1}, pressure = 30 N), we successfully fabricated silver electrode grid lines with excellent dimensional characteristics: width 18.68 ± 0.5 μm, height 9.44 ± 0.3 μm, achieving an aspect ratio of 0.50.

Data availability

The datasets generated during this study are fully available within the article.

Conflicts of interest

The authors declare that they have no known competing financial interests or personal relationships that could have influenced the work reported in this paper.

Acknowledgements

This research was funded by the Major Science and Technology project of Yunnan Province, Grant number 202402AB080005 and 202502AF080001; the Basic Research Project of Yunnan Province, Grant number 202501AS070110; and the Science and Technology projects of Yunnan Precious Metals Laboratory, Grant numbers YPML-2023050206 and YPML-20240502102.

References

1 D. Munoz-Martin, C. F. Brasz, Y. Chen, *et al.*, Laser-induced forward transfer of high-viscosity silver pastes, *Appl. Surf. Sci.*, 2016, **366**, 389–396.
2 F. Bonaccorso, A. Bartolotta, J. N. Coleman, *et al.*, 2D-Crystal-Based Functional Inks, *Adv. Mater.*, 2016, **28**(29), 6136–6166.
3 R. Li, H. Wang, Y. Tai, *et al.*, Influence of the properties of organic media in back-side silver pastes on the electrical performance of polycrystalline silicon solar cells, *RSC Adv.*, 2016, **6**(49), 43732–43739.
4 Q. Che, H. Yang, L. Lu, *et al.*, A new environmental friendly silver front contact paste for crystalline silicon solar cells, *J. Alloys Compd.*, 2013, **549**, 221–225.

5 H. W. Lin, C. P. Chang, W. H. Hwu and M. D. Ger, The rheological behaviors of screen-printing pastes, *J. Mater. Process. Technol.*, 2008, **197**(1–3), 284–291.
6 S. Tepner and A. Lorenz, Printing technologies for silicon solar cell metallization: A comprehensive review, *Prog. Photovoltaics*, 2023, **31**(6), 557–590.
7 S. Hemmati, D. P. Barkey and N. Gupta, Rheological behavior of silver nanowire conductive inks during screen printing, *J. Nanopart. Res.*, 2016, **18**(8), 1–11.
8 J. Zhang, Y. Cui and H. Wang, Optimization of viscosity and thixotropy for organic medium to achieve high photovoltaic conversion efficiency of silicon solar cells, *J. Renew. Sustain. Energy*, 2013, **5**(2), 1–12.
9 C. P. Hsu, R. H. Guo, C. C. Hua, *et al.*, Effect of polymer binders in screen printing technique of silver pastes, *J. Polym. Res.*, 2013, **20**, 1–8.
10 J. Qin, S. Bai, W. Zhang, *et al.*, Effects of organic medium on rheological properties of silver pastes for crystalline silicon solar cells, *Circ. World*, 2016, **42**(2), 77–83.
11 Y. Tian, S. Yu, W. Sun, *et al.*, Preparation of electronic pastes for high-precision screen printing: action mechanisms and synergistic effects of different polymer binders, *Surf. Interfaces*, 2025, **65**, 106525.
12 Y. Zhou, H. Tong, Y. Liu, *et al.*, Rheological effect on screen-printed morphology of thick film silver paste metallization, *J. Mater. Sci.: Mater. Electron.*, 2017, **28**, 5548–5553.
13 S. Thibert, J. Jourdan, B. Bechevet, *et al.*, Influence of silver paste rheology and screen parameters on the front side metallization of silicon solar cell, *Mater. Sci. Semicond. Process.*, 2014, **27**, 790–799.
14 A. S. K. Chunduri and M. Schmela, *Market Survey Screen Printers 2018*, Tai yang news, 2018.
15 W. M. Valentine and M. Mageto, Electrical and Structural Properties of Aluminium Doped tin Oxide Codoped with Sulphur for Solar Energy, *Energy Proc.*, 2016, **93**, 39–45.
16 C. Battaglia, J. Escarré, K. Söderström, *et al.*, Nanoimprint Lithography for High-Efficiency Thin-Film Silicon Solar Cells, *Nano Lett.*, 2011, **11**(2), 661–665.
17 K. Inukai, Y. Takahashi, K. Ri, *et al.*, Rheological analysis of ceramic pastes with ethyl cellulose for screen-printing, *Ceram. Int.*, 2015, **41**(4), 5959–5966.
18 S. Lee, U. Paik, S.-M. Yoon and J.-Y. Choi, Dispersant-ethyl cellulose binder interactions at the Ni particle-dihydroterpineol interface, *J. Am. Ceram. Soc.*, 2006, **89**(10), 3050–3055.
19 C. Xu and N. Willenbacher, How rheological properties affect fine-line screen printing of pastes: a combined rheological and high-speed video imaging study, *J. Coat. Technol. Res.*, 2018, **15**(6), 1401–1412.
20 L. Mo, Y. Zhang, L. Zhao, *et al.*, Effect of sub-micrometer sized silver particle on the performance of the front Ag paste for c-Si solar cells, *J. Alloys Compd.*, 2018, **742**, 256–262.
21 M. Vincent, V. K. Gopalakrishnan, S. Sivanandan, *et al.*, Factors influencing rheological characteristics of silver thick film paste and its correlation to multilayer ceramic processing, *Adv. Appl. Ceram.*, 2019, **118**(3), 106–113.
22 K. Inukai, Y. Takahashi, S. Murakami, *et al.*, Molecular weight dependence of ethyl cellulose adsorption behavior on (La, Sr)(Ti, Fe) O3− δ particles in organic solvent pastes and their printing properties, *Ceram. Int.*, 2014, **40**(8), 12319–12325.
23 Y. Hu, Z. Du, Y. Yao, *et al.*, Effects of organic additives on the microstructural, rheological and electrical properties of silver paste for LTCC applications, *J. Mater. Sci.: Mater. Electron.*, 2021, **32**(11), 14368–14384.
24 H. I. Hsiang, C. C. Chen, L. F. Fan, *et al.*, Rheological behaviors of silver conductive pastes with ethyl cellulose, *Circ. World*, 2020, **47**(1), 43–49.
25 C. Xu, M. Fieß and N. Willenbacher, Impact of wall slip on screen printing of front-side silver pastes for silicon solar cells, *IEEE J. Photovoltaics*, 2016, **7**(1), 129–135.
26 J. S. Jiang, J. E. Liang, H. L. Yi, *et al.*, Rheological fingerprints of time-evolving polymer-particle interaction and sol–gel transition in silver pastes, *J. Polym. Res.*, 2015, **22**, 1–11.
27 R. Faddoul, N. Reverdy-Bruas and J. Bourel, Silver content effect on rheological and electrical properties of silver pastes, *J. Mater. Sci.: Mater. Electron.*, 2012, **23**, 1415–1426.
28 M. Pospischil, K. Zengerle, J. Specht, *et al.*, Investigations of thick-film-paste rheology for dispensing applications, *Energy Proc.*, 2011, **8**, 449–454.
29 Y. Gao, J. Feng, F. Liu and Z. Liu, Effects of Organic Vehicle on the Rheological and Screen-Printing Characteristics of Silver Paste for LTCC Thick Film Electrodes, *Materials*, 2022, **15**(5), 1953.
30 K. Inukai, Y. Takahashi, K. Ri, *et al.*, Rheological analysis of ceramic pastes with ethyl cellulose for screen-printing, *Ceram. Int.*, 2015, **41**(4), 5959–5966.